

## Low-energy enhancement in the $\gamma$ -ray strength functions of $^{73,74}\text{Ge}$

T. Renström,<sup>1,\*</sup> H.-T. Nyhus,<sup>1</sup> H. Utsunomiya,<sup>2</sup> R. Schwengner,<sup>3</sup> S. Goriely,<sup>4</sup> A. C. Larsen,<sup>1</sup> D. M. Filipescu,<sup>5,6</sup> I. Gheorghe,<sup>5</sup> L. A. Bernstein,<sup>7</sup> D. L. Bleuel,<sup>7</sup> T. Glodariu,<sup>6</sup> A. Görge,<sup>1</sup> M. Guttormsen,<sup>1</sup> T. W. Hagen,<sup>1</sup> B. V. Kheswa,<sup>8</sup> Y.-W. Lui,<sup>9</sup> D. Negi,<sup>8,10</sup> I. E. Ruud,<sup>1</sup> T. Shima,<sup>11</sup> S. Siem,<sup>1</sup> K. Takahisa,<sup>11</sup> O. Tesileanu,<sup>5</sup> T. G. Tornyi,<sup>1,12</sup> G. M. Tveten,<sup>1</sup> and M. Wiedeking<sup>8</sup>

<sup>1</sup>*Department of Physics, University of Oslo, N-0316 Oslo, Norway*

<sup>2</sup>*Department of Physics, Konan University, Okamoto 8-9-1, Higashinada, Kobe 658-8501, Japan*

<sup>3</sup>*Institute of Radiation Physics, Helmholtz-Zentrum Dresden-Rossendorf, 01328 Dresden, Germany*

<sup>4</sup>*Institut d'Astronomie et d'Astrophysique, Université Libre de Bruxelles, Campus de la Plaine, CP-226, 1050 Brussels, Belgium*

<sup>5</sup>*ELI-NP, "Horia Hulubei" National Institute for Physics and Nuclear Engineering (IFIN-HH), 30 Reactorului, 077125 Bucharest-Magurele, Romania*

<sup>6</sup>*"Horia Hulubei" National Institute for Physics and Nuclear Engineering (IFIN-HH), 30 Reactorului, 077125 Bucharest-Magurele, Romania*

<sup>7</sup>*Lawrence Livermore National Laboratory, 7000 East Avenue, Livermore, California 94550-9234, USA*

<sup>8</sup>*iThemba LABS, P.O. Box 722, 7129 Somerset West, South Africa*

<sup>9</sup>*Cyclotron Institute, Texas A&M University, College Station, Texas 77843, USA*

<sup>10</sup>*Centre for Excellence in Basic Sciences, Vidyanagari Campus, Mumbai 400098, India*

<sup>11</sup>*Research Center for Nuclear Physics, Osaka University, Suita, Osaka 567-0047, Japan*

<sup>12</sup>*Institute of Nuclear Research of the Hungarian Academy of Sciences (MTA Atomki), Debrecen, Hungary*

(Received 18 October 2015; revised manuscript received 14 March 2016; published 2 June 2016)

The  $\gamma$ -ray strength functions and level densities of  $^{73,74}\text{Ge}$  have been extracted up to the neutron-separation energy  $S_n$  from particle- $\gamma$  coincidence data using the Oslo method. Moreover, the  $\gamma$ -ray strength function of  $^{74}\text{Ge}$  above  $S_n$  has been determined from photoneutron measurements; hence these two experiments cover the range of  $E_\gamma \approx 1\text{--}13$  MeV for  $^{74}\text{Ge}$ . The obtained data show that both  $^{73,74}\text{Ge}$  display an increase in strength at low  $\gamma$  energies. The experimental  $\gamma$ -ray strength functions are compared with  $M1$  strength functions deduced from average  $B(M1)$  values calculated within the shell model for a large number of transitions. The observed low-energy enhancements in  $^{73,74}\text{Ge}$  are adopted in the calculations of the  $^{72,73}\text{Ge}(n,\gamma)$  cross sections, where there are no direct experimental data. Calculated reaction rates for more neutron-rich germanium isotopes are shown to be strongly dependent on the presence of the low-energy enhancement.

DOI: [10.1103/PhysRevC.93.064302](https://doi.org/10.1103/PhysRevC.93.064302)

### I. INTRODUCTION

A good knowledge on how the atomic nucleus emits and absorbs photons is essential for the fundamental understanding of this many-faceted quantum system, as well as for a wide range of nuclear applications. To characterize the average, nuclear response to electromagnetic radiation, the  $\gamma$ -ray strength function ( $\gamma$ SF) [1] has proven to be a fruitful concept when the nucleus is excited to high energies and the density of quantum levels is high. There exists a wealth of information about the  $\gamma$ SF for nuclei above the neutron binding energy,  $S_n$ , predominantly from photoneutron experiments [2] and from the spectrum-fitting method [3]. For  $\gamma$  energies below  $S_n$  the information is more scarce, as it remains quite challenging to extract the  $\gamma$ SF experimentally in this energy range. For this region the Oslo method [4], the two-step cascade method [5] and a statistical treatment of nuclear-resonance fluorescence spectra [6] are frequently used.

For energies below  $\sim 3$  MeV, the  $\gamma$ SF of a nucleus is expected to correspond to the exponentially decreasing tail of the giant electric dipole resonance (GEDR). It therefore came as a surprise when a sizable low-energy enhancement in the  $\gamma$ SF, hereafter referred to as the *upbend*, was discovered below

3 MeV for  $^{56,57}\text{Fe}$  [7]. The  $\gamma$ SF measurement was performed at the Oslo Cyclotron Laboratory (OCL), using charged-particle reactions (and confirmed using the two-step cascade method). In the following years this phenomenon was observed in a wide range of nuclei using the Oslo method [8–14]. Recently, the upbend was also reported with a different experimental technique in  $^{95}\text{Mo}$  [15].

The physical mechanisms behind the upbend have been a puzzle for many years, but intense experimental and theoretical endeavors have recently led to results. Through angular-distribution measurements, it was demonstrated that the upbend is dominantly of dipole nature [16]. Furthermore, the authors of Ref. [17] suggested that the upbend is caused by thermal excitations in the continuum leading to enhanced low-energy  $E1$  transitions. Shell-model calculations performed in Refs. [18,19], on the other hand, show very strong  $M1$  transitions at low  $\gamma$ -ray energies. Moreover, it has been shown [20] that the presence of the upbend may enhance the  $r$ -process ( $n,\gamma$ ) reaction rates by a factor of 10–100.

Unfortunately, the various experimental techniques based on  $(\gamma,\gamma')$ ,  $(d,p)$ ,  $(^3\text{He},^3\text{He}'\gamma)$  reactions often give rise to large deviations in the  $\gamma$ SFs below  $S_n$ . Therefore, an international collaboration has been formed to investigate one specific nucleus as a test case. Germanium-74 was chosen, and four different experiments were performed:  $(^3\text{He},^3\text{He}'\gamma)$ ,  $(\alpha,\alpha'\gamma)$ ,  $(p,p'\gamma)$ , and  $(\gamma,\gamma')$ . In this work, we present results from

\*therese.renstrom@fys.uio.no

$^3\text{He}$ -induced reactions on  $^{74}\text{Ge}$  performed at the OCL, and data from a photoneutron experiment on  $^{74}\text{Ge}$  performed at NewSUBARU in Japan. In Sec. II, the experimental details and the data analysis of the two experiments are discussed. The normalization procedure of the OCL data is presented and a discussion of the resulting  $\gamma$ SFs is made in Sec. III. Shell-model calculations on the  $M1$  strength in  $^{73,74}\text{Ge}$  are presented in Sec. IV. Neutron-capture cross sections and reaction rates are shown in Sec. V. Finally, a summary and outlook can be found in Sec. VI.

## II. EXPERIMENTAL RESULTS

### A. The charged-particle experiment

The charged-particle experiment was performed at the OCL, where a beam of 38-MeV  $^3\text{He}$  particles with a current of  $\approx 0.5$  enA impinged on a self-supporting  $0.5$  mg/cm $^2$ -thick  $^{74}\text{Ge}$  target. The target was continuously irradiated for 7 days. About  $5 \times 10^6$  and  $2 \times 10^6$  particle- $\gamma$  coincidences were recorded in each of the two reaction channels of interest:  $^{74}\text{Ge}(^3\text{He},^3\text{He}'\gamma)$  and  $^{74}\text{Ge}(^3\text{He},\alpha\gamma)$ .

The charged outgoing particles were identified and their energies measured with the SiRi system [21], consisting of 64  $\Delta E$ - $E$  silicon telescopes, with thicknesses of 130 and 1550  $\mu\text{m}$ , respectively. SiRi was placed in the forward direction, covering angles from  $\theta = 40^\circ$ – $54^\circ$ , and with a solid angle coverage of  $\approx 6\%$  of  $4\pi$ . The  $\gamma$  rays were measured by the CACTUS array [22] consisting of 28 collimated  $5'' \times 5''$  NaI(Tl) detectors placed on a spherical frame surrounding the target and the particle detectors. The total efficiency of CACTUS is 15.2(1)% at  $E_\gamma = 1332.5$  keV. Using reaction kinematics, the initial excitation energy of the residual nucleus can be deduced from the energy of the outgoing particles detected in SiRi. The particle- $\gamma$  coincidence technique is used to assign each  $\gamma$  ray to a cascade depopulating a certain initial excitation energy in the residual nucleus.

Figure 1(a) shows the excitation energy- $\gamma$  matrix ( $E_\gamma, E$ ) of the  $^{74}\text{Ge}(^3\text{He},^3\text{He}'\gamma)$  reaction, where the  $\gamma$  spectra have been unfolded [23] with the response functions of CACTUS. The neutron-separation energy of  $^{74}\text{Ge}$  is reflected clearly in a drop in  $\gamma$  intensity at  $E \approx S_n = 10.196$  MeV. A relatively weak diagonal at  $E = E_\gamma$  reveals that the direct feeding to the ground state of spin/parity  $0^+$  is not particularly favored in this reaction. A second and third more pronounced diagonal represent direct decay to the  $2^+$  states of 596 and 1204 keV, respectively. These  $\gamma$  rays stem from primary transitions in the  $\gamma$  cascades.

We would like to study the energy distribution of all primary  $\gamma$  rays originating from various excitation energies and extract level density and  $\gamma$ SF simultaneously from this information. Using the unfolded ( $E_\gamma, E$ ) matrix, a primary  $\gamma$  matrix,  $P(E_\gamma, E)$ , as shown in Fig. 1(b), is constructed using the subtraction method of Ref. [24]. The basic assumption behind this method is that the  $\gamma$ -ray decay pattern from any excitation bin is independent of whether this bin was populated directly via the ( $^3\text{He},\alpha\gamma$ ) or ( $^3\text{He},^3\text{He}'\gamma$ ) reactions or indirectly via  $\gamma$  decay from higher excitation levels following the initial nuclear reaction. This assumption is fulfilled when states have the same relative probability to be populated by the two processes, because  $\gamma$  branching ratios are properties of the levels themselves.

Fermi's golden rule predicts that the decay probability may be factorized into two factors: the transition matrix between the initial  $|i\rangle$  and final states  $\langle f|$  and the density of final states  $\rho_f$  [25]:

$$\lambda_{i \rightarrow f} = \frac{2\pi}{\hbar} |\langle f|H'|i\rangle|^2 \rho_f. \quad (1)$$

Turning to our first generation  $\gamma$ -ray spectra  $P(E_\gamma, E)$  we realize that they are proportional to the decay probability from

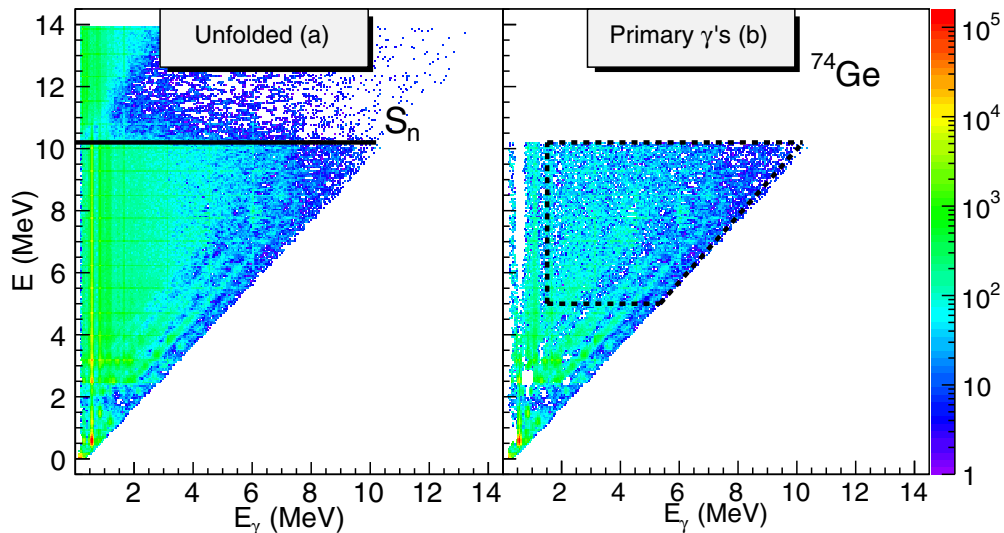


FIG. 1. (a) Excitation energy- $\gamma$  matrix from the  $^{74}\text{Ge}(^3\text{He},^3\text{He}'\gamma)^{74}\text{Ge}$  reaction. The NaI spectra are unfolded with the NaI response functions. (b) The first generation matrix from the same reaction. The area within the dashed lines is used in the further analysis.

$E$  to  $E_f$  and we may write the equivalent expression of Eq. (1) as

$$P(E_\gamma, E) \propto \mathcal{T}_{i \rightarrow f} \rho, \quad (2)$$

where  $\mathcal{T}_{i \rightarrow f}$  is the  $\gamma$ -ray transmission coefficient and  $\rho = \rho(E - E_\gamma)$  is the level density at the excitation energy  $E_f$  after the first  $\gamma$ -ray emission.

We notice that this expression does not allow us to simultaneously extract  $\mathcal{T}_{i \rightarrow f}$  and  $\rho$ . To do so, either one of the factorial functions must be known or some restrictions have to be introduced. Our restriction comes in the form of the Brink-Axel hypothesis [26,27]. The original hypothesis states that the GEDR can be built on any excited state and that the properties of the GEDR do not depend on the temperature of the nuclear state on which it is built. This hypothesis can be generalized to include not only the GEDR, but any kind of collective nuclear excitation and results in the assumption that primary  $\gamma$  spectra originating from the excitation energy  $E$  can be factorized into a  $\gamma$ -ray transmission coefficient,  $\mathcal{T}(E_\gamma)$ , which for the quasicontinuum only depends on the  $\gamma$ -transition energy  $E_\gamma$  [28], and into the level density  $\rho(E - E_\gamma)$  at the final level. We have now the following simple relation:

$$P(E_\gamma, E) \propto \mathcal{T}(E_\gamma) \rho(E - E_\gamma), \quad (3)$$

which permits a simultaneous extraction of the two functions from the first-generation matrix. At low excitation energies, the  $\gamma$  decay is, naturally, highly dependent on the individual initial and final states. This has been taken into consideration in our analysis, and we have excluded the  $\gamma$ -ray spectra originating from excitation energy bins below 3 MeV for  $^{73}\text{Ge}$  and 5 MeV for  $^{74}\text{Ge}$ . Also, a lower limit is set on the  $\gamma$  rays, where  $E_\gamma^{\min}$  is 1 and 1.5 MeV for  $^{73}\text{Ge}$  and  $^{74}\text{Ge}$ , respectively. In the range of  $E_\gamma < E_\gamma^{\min}$ , strong, discrete transitions are too heavily or too modestly subtracted in the first generation method and are thus excluded from further analysis.

At this point in the analysis, we have established the functional form of the level density and transmission coefficient. As demonstrated in Ref. [4], there exists an infinite set of solutions to Eq. (2), using transformations. The last stages of the analysis of the OCL data and the normalization procedure are described in Sec. III.

### B. The photoneutron experiment

The photoneutron cross section measurement was performed at the synchrotron radiation facility NewSUBARU in the Hyōgo Prefecture [29]. Here a wide range of quasi-monochromatic  $\gamma$  beams [30] are produced in head-on collisions between laser photons and relativistic electrons, so-called laser Compton scattering (LCS). The energy of the laser photons increases from a few eV to several MeV in the collision. In this experiment a 1.99-g/cm<sup>2</sup>-thick sample of  $^{74}\text{Ge}$ , enriched to 97.53%, was placed inside an aluminum container and irradiated with eight different  $\gamma$  beams with energies ranging from 10.4 to 12.7 MeV.

The  $^{74}\text{Ge}$  sample was mounted in the center of a  $4\pi$  neutron detection array comprised of 20  $^3\text{He}$  proportional counters embedded in a  $36 \times 36 \times 50$  cm<sup>3</sup> polyethylene moderator. The ring ratio technique [31] was used to measure the average

energies of the detected neutrons, and from this we establish the efficiency of the neutron detector as a function of neutron energy. A  $6'' \times 5''$  NaI(Tl) detector was used to measure the flux of the LCS beam. The detector was placed at the end of the  $\gamma$ -ray beam line. The intensity of  $\gamma$  rays hitting the  $^{74}\text{Ge}$  target was  $\approx 10^5$  s<sup>-1</sup>. The total number of  $\gamma$  rays on target for a certain beam energy was found using the pile-up method described in Ref. [32]. The almost monochromatic  $\gamma$  beams were monitored by a  $3.5'' \times 4.0''$  LaBr<sub>3</sub>(Ce) detector between every neutron measurement run. These spectra are reproduced using Geant4 [33] simulations and unfolded to extract the real energy profile of the incoming beam.

The  $(\gamma, n)$  cross section is given by

$$\int_{S_n}^{E_{\text{Max}}} n_\gamma(E_\gamma) \sigma(E_\gamma) dE_\gamma = \frac{N_n}{N_t N_\gamma \xi \epsilon_n g}, \quad (4)$$

where  $n_\gamma(E_\gamma)$  denotes the energy distribution of the  $\gamma$ -ray beam normalized to unity and  $\sigma(E_\gamma)$  is the photoneutron cross section to be determined. Furthermore,  $N_n$  represents the number of neutrons detected,  $N_t$  gives the number of target nuclei per unit area,  $N_\gamma$  is the number of  $\gamma$  rays incident on target,  $\epsilon_n$  represents the neutron detection efficiency, and  $\xi = (1 - e^{-\mu t})/(\mu t)$  gives a correction factor for a thick-target measurement, where  $t$  is the thickness of the target and  $\mu$  is the attenuation coefficient of the target. The factor  $g$  represents the fraction of the  $\gamma$  flux above  $S_n$ . Equation (4) is solved for the cross section using a Taylor expansion method described in Ref. [34]. In this way, we find cross sections for eight different energies, starting from 200 keV above  $S_n$  of  $^{74}\text{Ge}$ . The total uncertainties in the measurements are  $\approx 4.4\%$  [35]. The resulting  $^{74}\text{Ge}(\gamma, n)$  cross sections are shown in Fig. 2. We note that the newly measured data are lower than the data retrieved from a positron annihilation in-flight experiment by Carlos *et al.* [36] by  $\approx 30\%$ . The same trend has been reported by Berman *et al.* [37]. In the insert in Fig. 2, the difference in shape between the two data sets becomes more apparent; our newly measured cross sections vanish at  $\approx S_n$  as

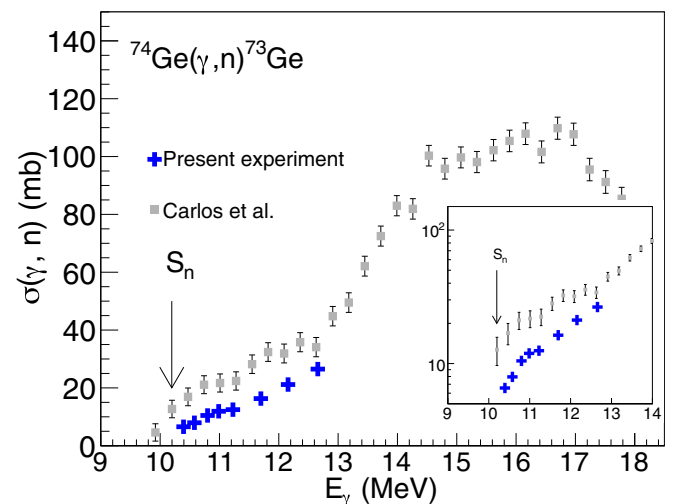


FIG. 2. Cross sections for the  $^{74}\text{Ge}(\gamma, n)$  reaction from the current experiment (blue crosses) together with existing photoneutron data [36].

expected, whereas the Carlos data exhibit a nonzero value in this range.

### III. NORMALIZATION OF THE OCL DATA

Once we have extracted the two vectors  $\rho(E - E_\gamma)$  and  $\mathcal{T}(E_\gamma)$  from the first generation matrix, we can construct infinitely many solutions [4] that give identical fits to the experimental data. The set of solutions are of the following form:

$$\tilde{\rho}(E - E_\gamma) = A \exp[\alpha(E - E_\gamma)] \rho(E - E_\gamma), \quad (5)$$

$$\tilde{\mathcal{T}}(E_\gamma) = B \exp(\alpha E_\gamma) \mathcal{T}(E_\gamma), \quad (6)$$

and it is necessary to determine the transformation coefficients  $A$ ,  $\alpha$ , and  $B$ , which gives solutions corresponding to the actual level densities and  $\gamma$ -transmission coefficients of  $^{73,74}\text{Ge}$ . To be able to do this, we take advantage of auxiliary data, mainly stemming from neutron-resonance experiments. This process of determining the coefficients and thus the physical solutions is what we refer to as *normalization* of our experimental data.

#### A. Level density

We start by establishing the normalized nuclear level densities (NLD) of  $^{73,74}\text{Ge}$ . This entails determining the two coefficients  $A$  and  $\alpha$  of Eq. (5). For this purpose we need two anchor points, i.e., two regions of excitation energy where there exist information on the NLD, either from experimental data or from theoretical calculations. A proper spacing between the anchor points is essential to ensure a reliable normalization. At low excitation energies, known, discrete levels can be used. The anchor points at low excitation energies of the two Ge isotopes are found simply by using the definition of NLD,  $\rho = \frac{\Delta N}{\Delta E}$ , where  $\Delta N$  is the number of levels in the  $\Delta E$  energy bin, using the same bin size as our experimental one, where  $\Delta E = 105$  keV. The level schemes of  $^{73,74}\text{Ge}$  are assumed to be close to complete up to excitation energies of 1.38 and 3.4 MeV, respectively [38], and we choose an area below these energies for normalization (see Fig. 3, where the arrows to the left show the area used in the case of  $^{74}\text{Ge}$ ).

The second anchor point is at higher energies, where the most reliable experimental data on the NLD comes from neutron-resonance experiments that provide average neutron spacings,  $D$ , in the area of the neutron-separation energy. In the case of  $^{73,74}\text{Ge}$ ,  $s$ -wave spacings,  $D_0$ , are given in both RIPL-3 [39] and the *Atlas of Neutron Resonances* of Mughabghab [40], from neutron capture on  $^{72}\text{Ge}$  and  $^{73}\text{Ge}$ . After careful consideration, we have chosen to use an average value of the two proposed sets of  $D_0$  values and uncertainties. The two main reasons for this choice are the following.

- (i) For  $^{73,74}\text{Ge}$  the  $D_0$  values from Ref. [40] are larger by 38% and 60%, respectively, than the values given in Ref. [39].
- (ii) Reference [40] presents a table of measured resonances. The experimental results that give the values listed in Ref. [39] are, to our knowledge, not presented in any peer-reviewed publication.

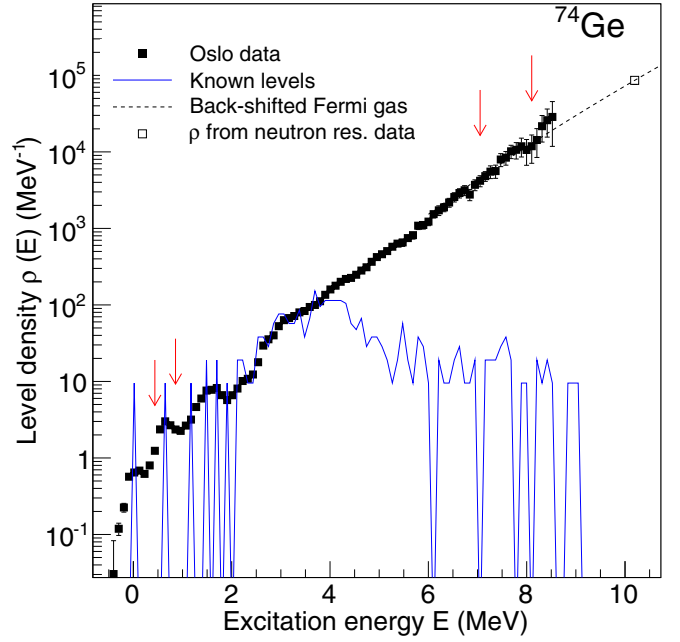


FIG. 3. Experimental level density of  $^{74}\text{Ge}$ . The data are normalized to known discrete levels at low excitation energy and to the level density extracted at  $S_n$  from neutron-capture resonance spacings  $D_0$ . The two sets of arrows indicate where the data are normalized.

The  $s$ -wave spacings can be expressed in terms of partial level densities:

$$D_0 = \frac{1}{\rho(S_n, I_t + 1/2, \pi_t) + \rho(S_n, I_t - 1/2, \pi_t)} \quad \text{for } I_t > 0, \quad (7)$$

$$= \frac{1}{\rho(S_n, 1/2, \pi_t)} \quad \text{for } I_t = 0, \quad (8)$$

where  $I_t$  and  $\pi_t$  are the spin and parity, respectively, of the target nucleus. From Eq. (8), we find that the measured level spacing  $D_0$  in the case of the  $^{72}\text{Ge}(n, \gamma)$  reaction corresponds to the density of  $\frac{1}{2}+$  states in  $^{73}\text{Ge}$  at  $S_n = 6.783$  MeV,  $\rho_{\frac{1}{2}+}(S_n)$ . From  $^{73}\text{Ge}(n, \gamma)$ , the density of  $4+$  and  $5+$  states of  $^{74}\text{Ge}$  at  $S_n = 10.196$  MeV,  $\rho_{4+,5+}(S_n)$ , can be estimated. Our experimental NLD represents the density of almost all accessible spins at  $S_n$ . From semiclassical calculations, we get  $I_{\max} \simeq 10\hbar$  for a  $^3\text{He}$  beam at 38 MeV. Due to the lower limits applied on  $E_\gamma$  (see Sec. II) in the extraction of  $\rho$  and  $\mathcal{T}$ , our NLDs reach only up to  $E \approx S_n - 1.5$  MeV. We need to make an interpolation between our data points and the NLD at  $S_n$ . The back-shifted Fermi gas model with the parametrization of Egidy and Bucurescu [41] has been chosen for this purpose (see Table I). Another option had been to use a constant temperature model for the interpolation as recommended in Ref. [42], but in this case where the gap between the last data point and  $S_n$  is so small the two types of interpolations give very similar results (see Ref. [43]). From this point in the analysis we carry out the normalization according to two different normalization schemes.

TABLE I. Parameters used in the normalization of NLD and  $\gamma$ SF.

Nucleus	$I_t^\pi$	$D_0$ (eV)	$S_n$ (MeV)	$\sigma(S_n)$	$a$ (MeV $^{-1}$ )	$E_1$ (MeV)	$\rho(S_n)_{\text{norm-1}}$ (MeV $^{-1}$ )	$\rho(S_n)_{\text{norm-2}}$ (MeV $^{-1}$ )	$\langle \Gamma_\gamma \rangle$ (meV)
$^{73}\text{Ge}$	$0^+$	1785(209)	6.783	3.66	9.00	-1.32	$156(35) \times 10^2$	23 521	195(50)
$^{74}\text{Ge}$	$9/2^+$	80.5(9)	10.196	3.77	9.70	0.71	$860(98) \times 10^2$	98 083	196(23)

### 1. norm-1

The main idea of this approach is to go from the spin- and parity-dependent NLD to the total NLD at  $S_n$ :

$$\rho_{\text{tot}}(S_n) = \sum_I \sum_\pi \rho(S_n, I, \pi). \quad (9)$$

This equation shows that we need information about the spin and parity distribution around the neutron-separation energy. These quantities are both notoriously difficult to measure experimentally for all spins and both parities at such high excitation energies. At this point two assumptions are made.

- (i) The spin dependence of the level density is given by the following statistical approximation [44,45]:

$$g(E, I) \simeq \frac{2I + 1}{2\sigma^2} \exp[-(I + 1/2)^2 / 2\sigma^2], \quad (10)$$

where  $I$  is the spin. The spin cutoff parameter,  $\sigma$ , is parametrized as recommended in Ref. [41]:

$$\sigma(E_x) = 0.391A^{0.675}(E_x - 0.5\text{Pa}'), \quad (11)$$

where  $A$  is the mass number,  $E_x$ , is the excitation energy and  $\text{Pa}'$  is the deuteron pairing energy as listed in Ref. [41]. The fact that in the case of  $^{74}\text{Ge}$  we know the density of  $4^+$  and  $5^+$  states that lie close to the center of the assumed spin distribution will most probably lead to a good estimation of the full spin distribution.

- (ii) There is an equipartition of parities at the neutron-separation energy for the two Ge isotopes. The assumption of parity symmetry at these high excitation energies for nuclei in this mass region is supported by Ref. [46].

We can now express the level density at  $S_n$  by [4]

$$\rho(S_n) = \frac{2\sigma^2}{D_0} \frac{1}{(I_t + 1) \exp[-(I_t + 1)^2 / 2\sigma^2] + I_t \exp[-I_t^2 / 2\sigma^2]}, \quad (12)$$

and we have found our second anchor point.

### 2. norm-2

Recent microscopic calculations [47–49] based on the Hartree-Fock-Bogolyubov (HFB) plus combinatorial (HFB + Comb) approach have been successful in calculating the NLDs of a wide range of nuclei. Such an approach provides the energy, spin, and parity dependence of the NLD. For flexibility, the calculated NLD can be normalized, if need be, to reproduce experimental  $s$ -wave spacings and the density of discrete levels at low excitation energies. These calculations have no *a priori* assumptions on the spin or parity distribution.

The microscopic calculations generally give a broad spin distribution with a center of gravity at quite high spins, and provide a higher NLD at  $S_n$  than norm-1 (see Table I).

We keep in mind that the different normalizations, norm-1 and norm-2, will lead to different slopes,  $\alpha$ , of the normalized level density, and because of their interconnection they also will determine the slope for the  $\gamma$ -transmission coefficient, see Eqs. (5) and (6).

In Fig. 4 the results of the two normalizations of the NLDs are presented; norm-1 and norm-2 give a lower and upper limit of the normalization of the two NLDs. We see that the discrete levels at low excitation energy are well reproduced and that

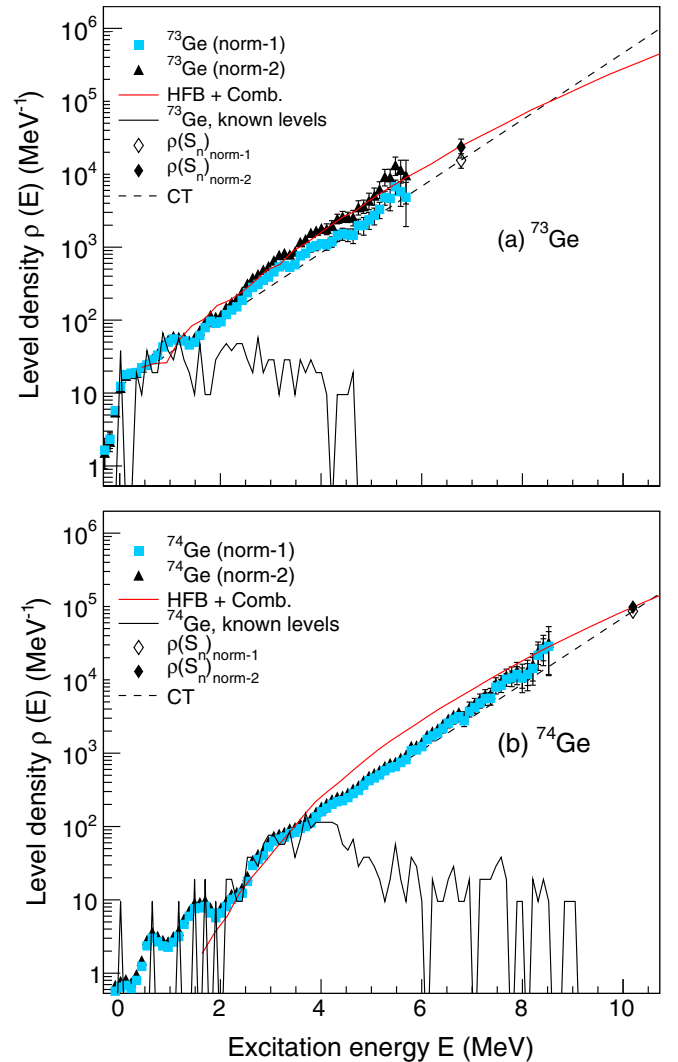


FIG. 4. Level density of (a)  $^{73}\text{Ge}$  and (b)  $^{74}\text{Ge}$  normalized according to norm-1 and norm-2.

the good statistics of the experiment yields small statistical errors.

It is seen that the unpaired neutron in  $^{73}\text{Ge}$  implies a higher NLD than for  $^{74}\text{Ge}$ . Another striking feature is the linearity of the NLD in log scale. This means that the NLD can be well described by the constant temperature expression [44,50]:

$$\rho_{\text{CT}}(E) = \frac{1}{T_{\text{CT}}} \exp\left(\frac{E - E_0}{T_{\text{CT}}}\right), \quad (13)$$

where  $T_{\text{CT}}$  is determined by the slope of  $\ln\rho(E)$ . This linearity has previously been observed for many nuclei and is described in detail in Refs. [42,51]. For  $^{73}\text{Ge}$  and  $^{74}\text{Ge}$ , the constant temperature parameters obtained for norm-1 data are  $T_{\text{CT}} = (0.95, 0.96)$  and  $E_0 = (-2.35, -0.7)$ , respectively.

### B. $\gamma$ -transmission coefficient and $\gamma$ SF

The normalization of the  $\gamma$ -transmission coefficient,  $\mathcal{T}(E_\gamma)$ , consists of determining the scaling factor  $B$  in Eq. (6) because  $\alpha$  is already determined. Average radiative widths of neutron resonances  $\langle\Gamma_\gamma\rangle$  are very important properties of  $\gamma$  decay from nuclear states at high excitation energy and can be used to normalize  $\mathcal{T}(E_\gamma)$ . We normalize according to [52]

$$\begin{aligned} &\langle\Gamma_\gamma(S_n, I_t \pm 1/2, \pi_t)\rangle \\ &= \frac{D_0}{4\pi} \int_{E_\gamma=0}^{S_n} dE_\gamma B \mathcal{T}(E_\gamma) \rho(S_n - E_\gamma) \\ &\quad \times \sum_{I=-1}^1 g(S_n - E_\gamma, I_t \pm 1/2 + I), \end{aligned} \quad (14)$$

where  $I_t$  and  $\pi_t$  are the spin and parity of the target nucleus in the  $(n, \gamma)$  reaction and  $\rho(S_n - E_\gamma)$  is the experimental level density.

The total average radiative widths are rather complex, depending on the  $\gamma$ -transmission coefficient, the NLD, and the spin distribution. An average of the listed experimental values of  $\langle\Gamma_\gamma\rangle$  from Refs. [39,40] is taken for  $^{74}\text{Ge}$ , giving  $\langle\Gamma_\gamma\rangle = 196(9)$  meV. The large number of resonances listed in Ref. [40] gives us confidence in the quite low uncertainty in this quantity. We also note that this value of  $\langle\Gamma_\gamma\rangle$  gives a good agreement with the newly measured  $(\gamma, n)$  data. Concerning the listed value of  $\langle\Gamma_\gamma\rangle$  for  $^{73}\text{Ge}$  in Ref. [40], we notice that this average value is only based on four experimental values, ranging between 120 and 230 meV, giving an average value of 150(35) meV. RIPL3 [39] lists a value of 162(50) meV. These values are 15%–30% lower than the average value for  $^{74}\text{Ge}$ . Considering the poor statistics of  $^{73}\text{Ge}$  compared to the case of  $^{74}\text{Ge}$ , we have chosen to set the  $\langle\Gamma_\gamma\rangle$  value of  $^{73}\text{Ge}$  to 195(50) meV, also to be consistent with the  $(\gamma, n)$  data for  $^{74}\text{Ge}$ . As for the NLDs, we follow here two parallel normalization schemes. Lastly, taking into account that the transitions between states in the quasicontinuum are dominantly of dipole type (see, e.g., Refs. [16,53]), the  $\gamma$ -transmission coefficient,  $\mathcal{T}(E_\gamma)$ , relates to the  $\gamma$ SF,  $f(E_\gamma)$ , in the following way [39]:

$$f(E_\gamma) = \frac{\mathcal{T}(E_\gamma)}{2\pi E_\gamma^3}. \quad (15)$$

We thus deduce the dipole strength from the normalized  $\gamma$ -transmission coefficient.

Coming back to the photoneutron cross sections, they are related to the  $\gamma$ SF,  $f(E_\gamma)$ , by

$$f(E_\gamma) = \frac{1}{3\pi^2 \hbar^2 c^2} \frac{\sigma(E_\gamma)}{E_\gamma}, \quad (16)$$

which can be directly compared with the Oslo data from the principle of detailed balance, giving  $f_{\text{up}} \approx f_{\text{down}}$  [39].

Now we are ready to present the  $\gamma$ SF below  $S_n$  together with the data points above  $S_n$  from the photoneutron experiment. The  $\gamma$ SFs of  $^{73,74}\text{Ge}$  from the two normalization methods, norm-1 and norm-2, are shown in Fig. 5. The error bars of the data points include statistical errors and propagated systematic errors from the unfolding and the primary  $\gamma$ -ray extraction.

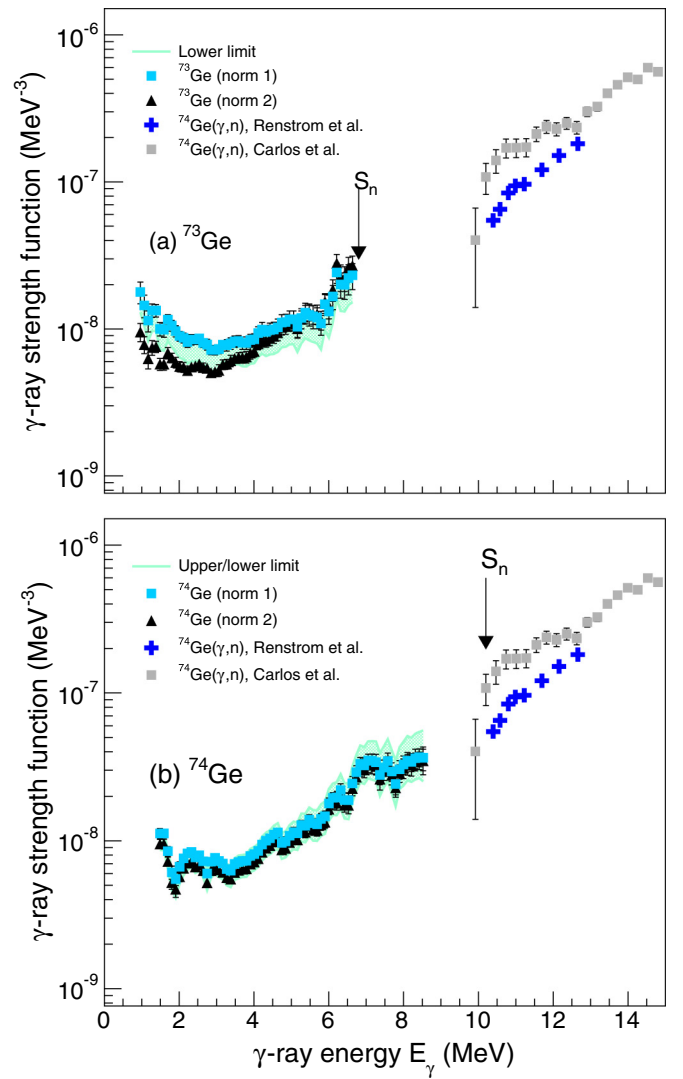


FIG. 5.  $\gamma$ SF for the different normalization procedures together with photoneutron data on  $^{74}\text{Ge}$  from the present experiment and from already existing photoneutron data from Ref. [36] for (a)  $^{73}\text{Ge}$  and (b)  $^{74}\text{Ge}$ . Note that  $^{74}\text{Ge}$   $\gamma$ SF above  $S_n$  has been compared with both  $^{73,74}\text{Ge}$  data from the current experiment. The green lines represent the upper and lower limits of norm-1.

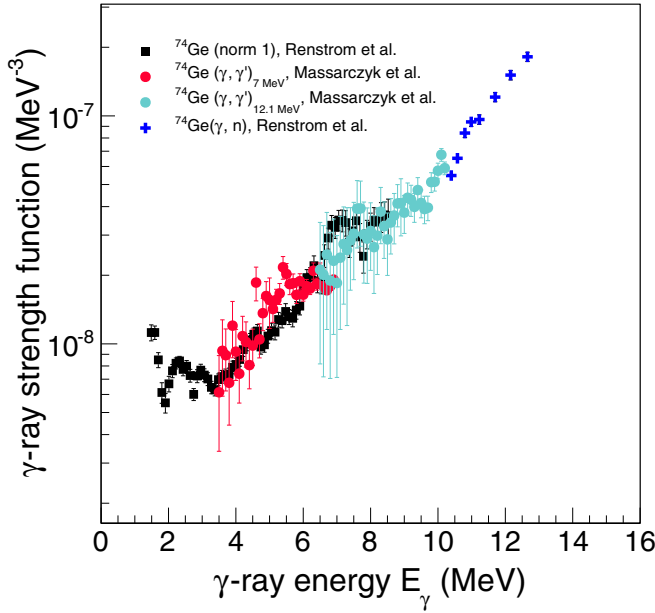


FIG. 6.  $\gamma$ SF of  $^{74}\text{Ge}$  obtained from photon scattering reactions utilizing electron beams of 7 and 12.1 MeV (red and green circles, respectively) [56], from a statistical analysis of primary  $\gamma$ -ray spectra (black squares), and from  $(\gamma, n)$  reactions (blue crosses).

Details of the error analysis are given in Ref. [4]. Systematic errors originating from the normalization process are indicated as upper and lower limits. The systematic errors are thoroughly discussed in Ref. [54]. We notice that norm-2 gives lower and steeper  $\gamma$ SFs than norm-1 in the case of  $^{73}\text{Ge}$ , but in the case of  $^{74}\text{Ge}$  the two normalization schemes give very similar results. The  $\gamma$ SFs below  $S_n$  are in both cases in good agreement with the new photo-neutron data on  $^{74}\text{Ge}$ .

We observe a possible resonancelike structure centered at  $\approx 7$  MeV. This has also been observed in the  $^{74}\text{Ge}(\alpha, \alpha')^{74}\text{Ge}$  reaction and interpreted as a Pygmy dipole resonance [55]. Strength functions from the  $^{74}\text{Ge}(\gamma, \gamma')$  experiment are in very good agreement with the results presented here, as shown in Fig. 6. We also see that both the  $\gamma$ SFs of  $^{73,74}\text{Ge}$  are increasing at decreasing  $\gamma$ -ray energies below  $\sim 3$  MeV. This finding is expected from the results of Ref. [57], where the  $\gamma$ SF of  $^{76}\text{Ge}$  was reported to show a similar upbend. In the following, we compare our data with calculations of the  $M1$  strength.

#### IV. SHELL-MODEL CALCULATIONS OF THE $M1$ STRENGTH

We have performed shell-model calculations by means of the code RITSSCHIL [58] using a model space composed of the  $(0f_{5/2}, 1p_{3/2}, 1p_{1/2}, 0g_{9/2})$  proton orbits and the  $(1p_{1/2}, 0g_{9/2}, 1d_{5/2})$  neutron orbits relative to a  $^{66}\text{Ni}$  core. This configuration space is analogous to the one applied in an earlier study of  $M1$  strength functions in  $^{94,95,96}\text{Mo}$  and  $^{90}\text{Zr}$  [18]. In the present calculations for  $^{73,74}\text{Ge}$ , four protons were allowed to be lifted from the  $fp$  shell to the  $0g_{9/2}$  orbit and two neutrons from the  $1p_{1/2}$  orbit to the  $0g_{9/2}$  orbit. This resulted in dimensions up to 11 400. For comparison,  $M1$  strength functions were deduced

also for the neutron-rich isotope  $^{80}\text{Ge}$ . In these calculations, one neutron could be excited from the  $0g_{9/2}$  orbit to the  $1d_{5/2}$  orbit. We note here that the restricted model space does not fully reproduce the collectivity in the near-yrast states of  $^{74}\text{Ge}$ . However, the calculations give an approach to the characteristics of  $M1$  transitions between excited states above the yrast line [18,59].

The calculations included states with spins from  $I = 0$  to 10. For each spin the lowest 40 states were calculated. Reduced transition probabilities  $B(M1)$  were calculated for all transitions from initial to final states with energies  $E_f < E_i$  and spins  $I_f = I_i$  and  $I_i \pm 1$ . For the minimum and maximum  $I_i$ , the cases  $I_f = I_i - 1$  and  $I_f = I_i + 1$ , respectively, were excluded. This resulted in more than 23 800  $M1$  transitions for each parity  $\pi = +$  and  $\pi = -$ , which were sorted into 100-keV bins according to their transition energy  $E_\gamma = E_i - E_f$ . The average  $B(M1)$  value for one energy bin was obtained as the sum of all  $B(M1)$  values divided by the number of transitions within this bin.

The  $M1$  strength functions were deduced using the relation

$$f_{M1}(E_\gamma) = 16\pi/9(\hbar c)^{-3}\overline{B}(M1, E_\gamma)\rho(E_i). \quad (17)$$

They were calculated by multiplying the  $B(M1)$  value in  $\mu_N^2$  of each transition with  $11.5473 \times 10^{-9}$  times the level density at the energy of the initial state  $\rho(E_i)$  in  $\text{MeV}^{-1}$  and deducing averages in energy bins as done for the  $\overline{B}(M1)$  values (see above). The level densities  $\rho(E_i, \pi)$  were determined by counting the calculated levels within energy intervals of 1 MeV for the two parities separately. The strength functions obtained for the two parities were subsequently added. Gates were put on the excitation energy  $E_x$ , corresponding to the ones applied in the analysis of the experimental data (see Sec. II). The resulting  $M1$  strength functions for  $^{73,74}\text{Ge}$  are shown in Fig. 7.

The calculated  $M1$  strength function shows a low-energy enhancement similar to that of the  $M1$  strength functions calculated for the neighboring nuclei  $^{94,95,96}\text{Mo}$  and  $^{90}\text{Zr}$  [18]

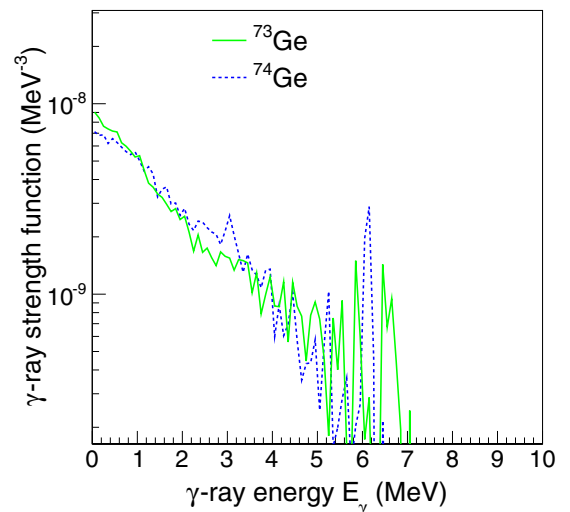


FIG. 7. Shell-model calculations of the  $M1$  component of the  $\gamma$ SF of  $^{74}\text{Ge}$  (blue dashed line) and  $^{73}\text{Ge}$  (green solid line).

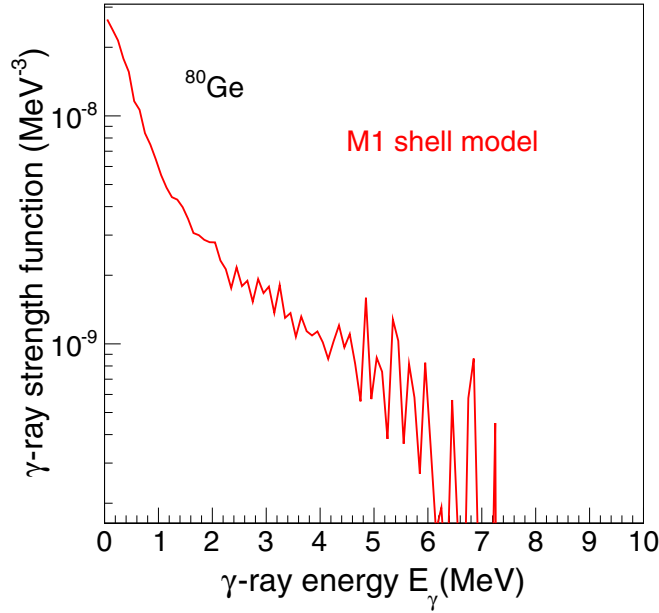


FIG. 8. Shell-model calculations of the  $M1$  component of the  $\gamma$ SF of  $^{80}\text{Ge}$ .

and for  $^{56,57}\text{Fe}$  [19]. However, the slope is not as steep as in the nuclides close to  $N = 50$  [18]. The  $M1$  strength function calculated for the  $N = 48$  isotope  $^{80}\text{Ge}$  is shown in Fig. 8. One sees that the slope of this is steeper than that of  $^{73,74}\text{Ge}$  and reaches larger values toward  $E_\gamma = 0$ . The dominating configurations of states in  $^{73}\text{Ge}$  linked by transitions with large  $B(M1)$  values are of the type  $\pi[(0f_{5/2}1p_{3/2})^4]\nu(1p_{1/2}^{-2}0g_{9/2}^3)$  for positive-parity states and  $\pi[(0f_{5/2}1p_{3/2})^4]\nu(1p_{1/2}^{-1}0g_{9/2}^2)$  for negative-parity states. In  $^{74}\text{Ge}$ , the configurations are analogous, including one  $0g_{9/2}$  neutron more. In addition, configurations of the type  $\pi[(0f_{5/2}1p_{3/2})^4]\nu(0g_{9/2}^2)$  contribute for positive parity. The corresponding configurations in  $^{80}\text{Ge}$  are  $\pi[(0f_{5/2}1p_{3/2})^4]\nu(0g_{9/2}^8)$  and  $\pi[(0f_{5/2}1p_{3/2})^4]\nu(0g_{9/2}^71d_{5/2}^1)$  for positive-parity states and  $\pi[(0f_{5/2}1p_{3/2})^30g_{9/2}^1]\nu(0g_{9/2}^8)$  and  $\pi[(0f_{5/2}1p_{3/2})^30g_{9/2}^1]\nu(0g_{9/2}^71d_{5/2}^1)$  for negative-parity states.

## V. CALCULATIONS OF $(n, \gamma)$ CROSS SECTIONS AND REACTION RATES

The measured NLD and the  $\gamma$ SF together with the nucleon-nucleus optical potential, assuming a compound reaction, can now be applied to calculate the neutron-capture cross section. It has been shown that using the experimental NLD and  $\gamma$ SF extracted using the Oslo method as input for  $(n, \gamma)$  cross-section calculations gives a very good agreement with experimental cross-section data [60]. In this work, we focus on the cross sections  $^{72}\text{Ge}(n, \gamma)^{73}\text{Ge}$  and  $^{73}\text{Ge}(n, \gamma)^{74}\text{Ge}$ .

It is interesting to notice that both Refs. [61] and [62] list  $^{72,73}\text{Ge}$  as amongst the very few of the 277 stable isotopes that, at present, lack  $(n, \gamma)$  cross-section data. Based on our new data on  $^{73,74}\text{Ge}$ , we can provide a semiexperimental capture reaction cross section. The reaction code TALYS-1.6 [63] is used

to perform the calculations. In the case of the neutron-nucleus optical potential we use the Koning and Delaroche model [64]. We have also tested the Jeukenne-Lejeune-Mahaux type of potential [65]. We find that, for typical  $s$ -process temperatures, the effect is  $\approx 16\%$ , which is well within our other systematic uncertainties. Based on the present status of the discussion of the electromagnetic character of the upbend, e.g., whether it is of the  $E1$  type or the  $M1$  type, we treat the input  $\gamma$ SF in two ways.

- (i) The upbend of the  $\gamma$ SF is described by the exponential function

$$f_{\text{up}}(E_\gamma) = C \exp[-\eta E_\gamma]. \quad (18)$$

The low-energy enhancement is considered to be of the  $M1$  type, supported by recent publications [18,19] and the present shell-model calculations. This is combined with Quasiparticle Random Phase Approximation (QRPA) calculations of the  $E1$  strength from Ref. [66] and a standard treatment of the  $M1$  spin-flip resonance as described in the TALYS documentation [63]. This combined function represents the  $\gamma$ SF input.

- (ii) We give measured experimental points of the  $\gamma$ SF as input and assume that all the strength is of the  $E1$  type, in accordance with Ref. [17].

The  $\gamma$ SFs of (i) and (ii) are both combined with two prescriptions for NLD: the one resulting from norm-1 and the pure HFB + combinatorial one from Ref. [49], the uncertainties of the  $D_0$  values and the  $\langle \Gamma_\gamma \rangle$  values being taken into account.

In Fig. 9(a) and 9(b), we show the upper and lower limits obtained using all normalizations of the  $\gamma$ SFs, as shown in Fig. 5, and the constant-temperature NLD. In Fig. 9(c) we test the impact of varying the electromagnetic character of the upbend in the  $\gamma$ SF, using again the constant-temperature NLD. The  $E1$  type gives on average 33% higher cross section than assuming an  $M1$  character. In Fig. 9(d) we keep the  $\gamma$ SF constant and vary the NLD prescription. The microscopic NLD gives on average a cross section that is 38% higher than that of the experimentally constrained NLD. Finally we combine all the variations and present our final error bands in Fig. 10.

The corresponding astrophysical Maxwellian-averaged cross sections amount to  $\langle \sigma \rangle = 66(13)$  and  $294(78)$  mb for  $^{72}\text{Ge}(n, \gamma)$  and  $^{73}\text{Ge}(n, \gamma)$ , respectively, at  $k_B T = 30$  keV (i.e., a temperature of  $T = 3.5 \times 10^8$  K), and agree well with the previous theoretical values recommended by Bao *et al.* [62] at  $\langle \sigma \rangle = 73(7)$  and  $243(47)$  mb, respectively.

### A. Reaction rates of neutron-rich Ge isotopes

It has previously been shown that the upbend can have a significant effect on the neutron-capture cross section of exotic neutron-rich nuclei [20]. Naturally, it is an open question whether the upbend exists in neutron-rich Ge isotopes (Ref. [57] reports a similar strength of the upbend in the  $\gamma$ SF of the slightly more neutron-rich isotope  $^{76}\text{Ge}$ ). The shell-model calculations of the  $^{80}\text{Ge}$   $M1$   $\gamma$ SF support the assumption



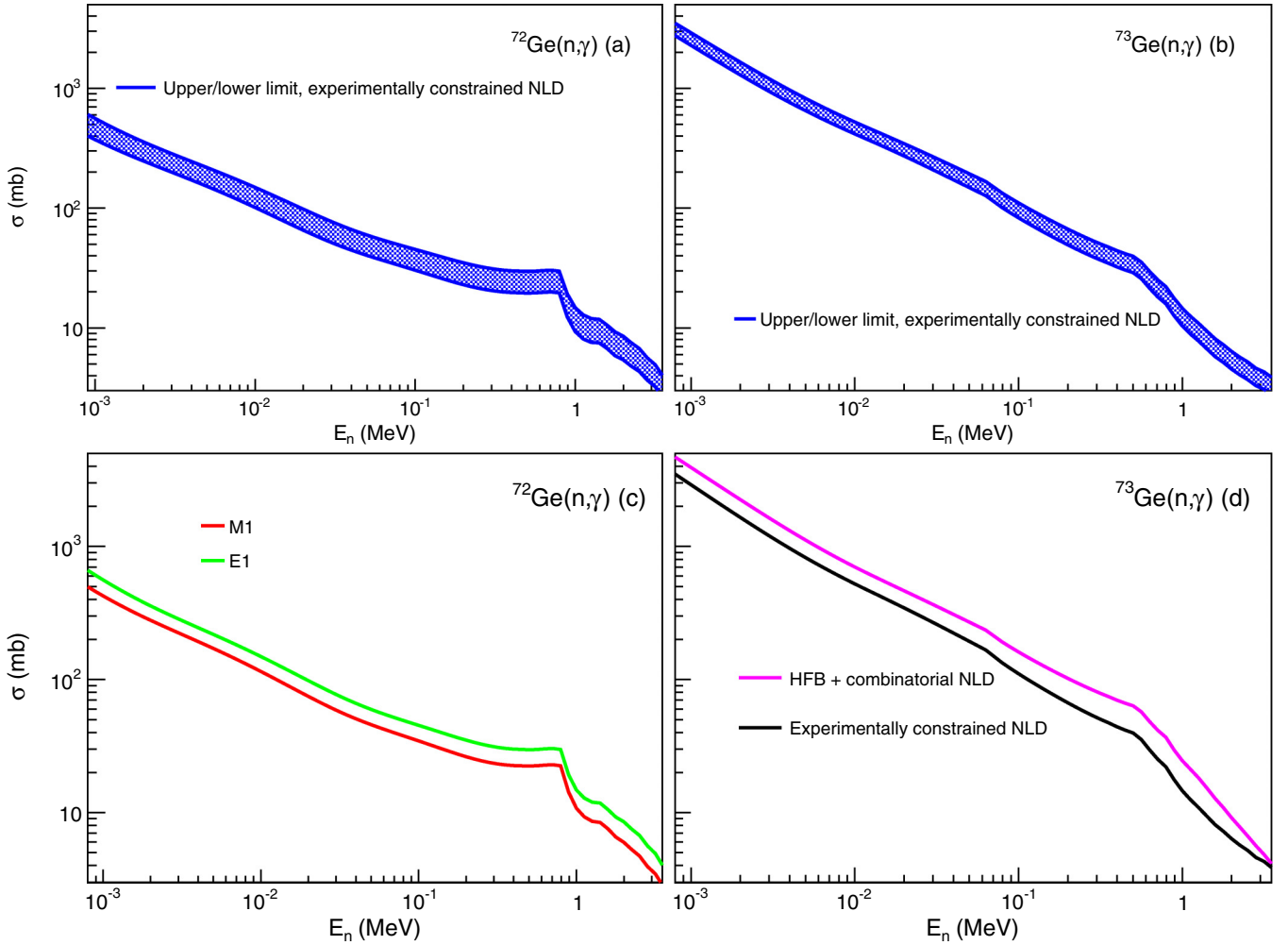


FIG. 9. Neutron capture cross section as a function of neutron energy for the  $^{72}\text{Ge}(n,\gamma)^{73}\text{Ge}$  and  $^{73}\text{Ge}(n,\gamma)^{74}\text{Ge}$  reactions. The calculations are performed using TALYS. In panels (a) and (b) resulting  $(n,\gamma)$  cross sections from using the  $\gamma$ SFs from Fig. 5 combined with the experimentally constrained NLD, are shown. In panel (b) the electromagnetic type of the  $\gamma$ SF is either  $E1$  or  $M1$ , while the level density type is kept constant. In panel (d) the level density input is varied, while the  $\gamma$ SF input is kept constant. See text for details.

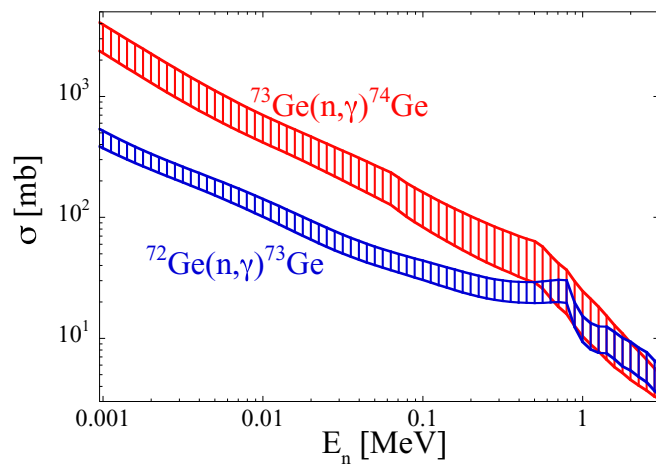


FIG. 10. Final neutron-capture cross sections for the  $^{72}\text{Ge}(n,\gamma)^{73}\text{Ge}$  and  $^{73}\text{Ge}(n,\gamma)^{74}\text{Ge}$  reactions including all uncertainties.

of a persisting upbend for neutron-rich Ge isotopes. In the following we assume that the upbend remains as strong in isotopes approaching the neutron drip line as observed in  $^{73,74}\text{Ge}$ . A fit to the  $^{74}\text{Ge}$   $\gamma$ SF data give the parameters  $(C,\eta) = (4 \times 10^{-8}, 0.99)$  in Eq. (18). These parameters for the upbend have been applied to the neutron-rich Ge isotopes. We calculate the ratio of the reaction rates including and excluding the upbend for temperatures corresponding to two proposed  $r$ -process sites [67]: a cold  $r$ -process in neutron star mergers and a hot  $r$ -process in the neutrino-driven wind of core-collapse supernovae. As we go to neutron-rich nuclei we rely on theoretical calculations of the  $S_n$ , NLD, and  $\gamma$ SF, because they are at this point experimentally inaccessible. Some uncertainties arise, especially from the mass model used to establish  $S_n$ . The inputs used in the TALYS calculations of the astrophysical reaction rates in this case are the following: for the mass, the Skyrme-HFB mass model of Ref. [68]; for the NLD, the HFB + Comb model [49]; and for the  $E1$   $\gamma$ SF, the HFB + QRPA model [69]. For the  $M1$  spin-flip resonance the standard TALYS treatment has been applied [39].

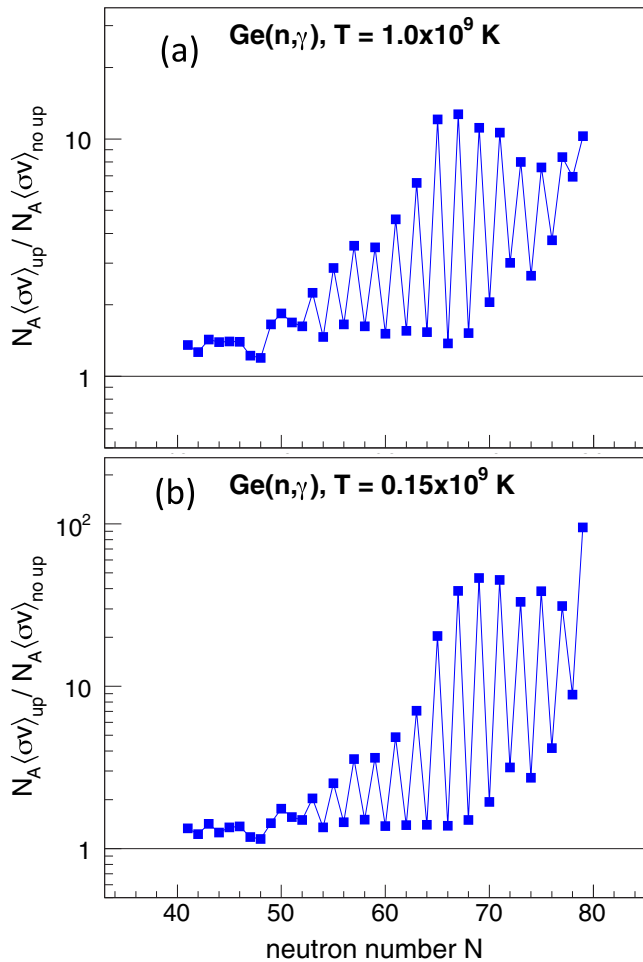


FIG. 11. Ratio of Maxwellian-averaged  $(n,\gamma)$  reaction rates including and excluding the upbend for the Ge isotopic chain up to the neutron drip line for temperatures (a)  $T = 1$  GK and (b)  $T = 0.15$  GK.

Calculations for a hot astrophysical environment of  $T = 1.0$  GK are shown in Fig. 11(a). Odd-even staggering effects are strong, reflecting the difference in the neutron-separation energy of isotopes with odd and even neutron numbers. The sensitive energy range of the  $\gamma$ SF in the neutron-capture reaction is situated typically a few MeV below  $S_n$ , corresponding to the upbend region for the extremely neutron-rich odd Ge isotopes. As expected, we see that the influence of the upbend becomes more important as the number of neutrons increases.

The maximum increase for the extremely neutron-rich nuclei is approximately a factor of 15 for the case of  $T = 1.0$  GK. Figure 11(b) shows the calculated reaction rates for the case of a cold  $r$ -process with  $T = 0.15$  GK. For this temperature, an increase of a factor of  $\approx 60$ – $70$  in the reaction rates is seen for the most neutron-rich isotopes. Even for more moderately neutron-rich nuclei, an increase of a factor of 2 can be observed. Hence, we conclude that the impact of the upbend on the  $(n,\gamma)$  reaction rates could be significant for the Ge case, as already shown in Ref. [20].

## VI. SUMMARY

The NLDs and  $\gamma$ SFs of  $^{73,74}\text{Ge}$  in the energy range below  $S_n$  have been extracted from particle- $\gamma$  coincidence data using the Oslo method. Moreover, the  $\gamma$ SF above  $S_n$  of  $^{74}\text{Ge}$  has been deduced from a photoneutron experiment. A low-energy enhancement in the  $\gamma$ SF was observed in both nuclei. Shell-model calculations on  $^{74}\text{Ge}$  indicate that the enhancement is (at least partly) due to  $M1$  transitions. The neutron-capture cross sections  $^{72}\text{Ge}(n,\gamma)$  and  $^{73}\text{Ge}(n,\gamma)$  could for the first time be experimentally constrained using our new data as input. The effect of the upbend on the astrophysical reaction rates was investigated and was shown to be significant for neutron-rich isotopes.

## ACKNOWLEDGMENTS

The authors thank J. C. Müller, E. A. Olsen, A. Semchenkov, and J. Wikne at the Oslo Cyclotron Laboratory for providing excellent experimental conditions and the LBNL for providing the  $^{74}\text{Ge}$  target used in the OCL experiment. Part of this work was supported by the Research Council of Norway under Grant No. 210007. A.C.L. acknowledges financial support from the Research Council of Norway under Grant No. 205528 and from the ERC-STG-2014 under Grant No. 637686. Part of this work was supported by the National Research Foundation of South Africa under Contracts No. 92789 and No. 78766. D.M.F., O.T., and I.G. acknowledge financial support from the Extreme Light Infrastructure Nuclear Physics (ELI-NP) Phase I, a project cofinanced by the Romanian Government and the European Union through the European Regional Development Fund (425/12.12.2012, POS CCE, ID 1334 SMIS-CSNR 40741). S.G. acknowledges the financial support from the F.N.R.S. Part of this work was performed under the auspices of the U.S. Department of Energy by Lawrence Livermore National Laboratory under Contract No. DE-AC52-07NA27344.

[1] G. A. Bartholomew, E. D. Earle, A. J. Ferguson, J. W. Knowles, and M. A. Lone, *Adv. Nucl. Phys.* **7**, 229 (1973).  
 [2] S. S. Dietrich and B. L. Berman, *At. Data Nucl. Data Tables* **38**, 199 (1988).  
 [3] A. Schiller and M. Thoennessen, *At. Data Nucl. Data Tables* **93**, 549 (2007).  
 [4] A. Schiller, L. Bergholt, M. Guttormsen, E. Melby, J. Rekstad, and S. Siem, *Nucl. Instrum. Methods Phys. Res., Sect. A* **447**, 498 (2000).

[5] A. M. Hoogenboom, *Nucl. Instrum. Methods* **3**, 57 (1958).  
 [6] G. Rusev, R. Schwengner, F. Dönau, M. Erhard, E. Grosse, A. R. Junghans, K. Kosev, K. D. Schilling, A. Wagner, F. Bečvář, and M. Krtička, *Phys. Rev. C* **77**, 064321 (2008).  
 [7] A. Voinov, E. Algin, U. Agvaanluvsan, T. Belgya, R. Chankova, M. Guttormsen, G. E. Mitchell, J. Rekstad, A. Schiller, and S. Siem, *Phys. Rev. Lett.* **93**, 142504 (2004).

- [8] A. C. Larsen, M. Guttormsen, R. Chankova, F. Ingebretsen, T. Lönnroth, S. Messelt, J. Rekstad, A. Schiller, S. Siem, N. U. H. Syed, and A. Voinov, *Phys. Rev. C* **76**, 044303 (2007).
- [9] A. Bürger, A. C. Larsen, S. Hilaire, M. Guttormsen, S. Harissopulos, M. Kmiecik, T. Konstantinopoulos, M. Krtička, A. Lagoyannis, T. Lönnroth, K. Mazurek, M. Norrby, H. T. Nyhus, G. Perdikakis, S. Siem, A. Spyrou, and N. U. H. Syed, *Phys. Rev. C* **85**, 064328 (2012).
- [10] A. C. Larsen, S. Goriely, A. Bürger, M. Guttormsen, A. Görgen, S. Harissopulos, M. Kmiecik, T. Konstantinopoulos, A. Lagoyannis, T. Lönnroth, K. Mazurek, M. Norrby, H. T. Nyhus, G. Perdikakis, A. Schiller, S. Siem, A. Spyrou, N. U. H. Syed, H. K. Toft, G. M. Tveten, and A. Voinov, *Phys. Rev. C* **85**, 014320 (2012).
- [11] N. U. H. Syed, A. C. Larsen, A. Bürger, M. Guttormsen, S. Harissopulos, M. Kmiecik, T. Konstantinopoulos, M. Krtička, A. Lagoyannis, T. Lönnroth, K. Mazurek, M. Norby, H. T. Nyhus, G. Perdikakis, S. Siem, and A. Spyrou, *Phys. Rev. C* **80**, 044309 (2009).
- [12] M. Guttormsen, A. C. Larsen, A. Bürger, A. Görgen, S. Harissopulos, M. Kmiecik, T. Konstantinopoulos, M. Krtička, A. Lagoyannis, T. Lönnroth, K. Mazurek, M. Norrby, H. T. Nyhus, G. Perdikakis, A. Schiller, S. Siem, A. Spyrou, N. U. H. Syed, H. K. Toft, G. M. Tveten, and A. Voinov, *Phys. Rev. C* **83**, 014312 (2011).
- [13] A. C. Larsen, R. Chankova, M. Guttormsen, F. Ingebretsen, S. Messelt, J. Rekstad, S. Siem, N. U. H. Syed, S. W. Ødegård, T. Lönnroth, A. Schiller, and A. Voinov, *Phys. Rev. C* **73**, 064301 (2006).
- [14] M. Guttormsen, R. Chankova, U. Agvaanluvsan, E. Algin, L. A. Bernstein, F. Ingebretsen, T. Lönnroth, S. Messelt, G. E. Mitchell, J. Rekstad, A. Schiller, S. Siem, A. C. Sunde, A. Voinov, and S. Ødegård, *Phys. Rev. C* **71**, 044307 (2005).
- [15] M. Wiedeking, L. A. Bernstein, M. Krtička, D. L. Bleuel, J. M. Allmond, M. S. Basunia, J. T. Burke, P. Fallon, R. B. Firestone, B. L. Goldblum, R. Hatarik, P. T. Lake, I.-Y. Lee, S. R. Leshner, S. Paschalis, M. Petri, L. Phair, and N. D. Scielzo, *Phys. Rev. Lett.* **108**, 162503 (2012).
- [16] A. C. Larsen, N. Blasi, A. Bracco, F. Camera, T. K. Eriksen, A. Görgen, M. Guttormsen, T. W. Hagen, S. Leoni, B. Million, H. T. Nyhus, T. Renstrøm, S. J. Rose, I. E. Ruud, S. Siem, T. Tornyi, G. M. Tveten, A. V. Voinov, and M. Wiedeking, *Phys. Rev. Lett.* **111**, 242504 (2013).
- [17] E. Litvinova and N. Belov, *Phys. Rev. C* **88**, 031302(R) (2013).
- [18] R. Schwengner, S. Frauendorf, and A. C. Larsen, *Phys. Rev. Lett.* **111**, 232504 (2013).
- [19] B. A. Brown and A. C. Larsen, *Phys. Rev. Lett.* **113**, 252502 (2014).
- [20] A. C. Larsen and S. Goriely, *Phys. Rev. C* **82**, 014318 (2010).
- [21] M. Guttormsen, A. Bürger, T. E. Hansen, and N. Lietaer, *Nucl. Instrum. Methods Phys. Res., Sect. A* **648**, 168 (2011).
- [22] M. Guttormsen, A. Ataç, G. Løvholden, S. Messelt, T. Ramsøy, J. Rekstad, T. F. Thorsteinsen, T. S. Tveter, and Z. Zelazny, *Phys. Scr.*, **T 32**, 54 (1990).
- [23] M. Guttormsen, T. S. Tveter, L. Bergholt, F. Ingebretsen, and J. Rekstad, *Nucl. Instrum. Methods Phys. Res., Sect. A* **374**, 371 (1996).
- [24] M. Guttormsen, T. Ramsøy, and J. Rekstad, *Nucl. Instrum. Methods Phys. Res., Sect. A* **255**, 518 (1987).
- [25] E. Fermi, *Nuclear Physics* (University of Chicago, Chicago, 1950).
- [26] D. M. Brink, Ph.D. thesis, Oxford University, 1955.
- [27] P. Axel, *Phys. Rev.* **126**, 671 (1962).
- [28] M. Guttormsen, A. C. Larsen, A. Görgen, T. Renstrøm, S. Siem, T. G. Tornyi, and G. M. Tveten, *Phys. Rev. Lett.* **116**, 012502 (2016).
- [29] S. Amano, K. Horikawa, K. Ishihara, S. Miyamoto, T. Hayakawa, T. Shizuma, and T. Mochizuki, *Nucl. Instrum. Methods Phys. Res., Sect. A* **602**, 337 (2009).
- [30] K. Horikawa, S. Miyamoto, S. Amano, and T. Mochizuki, *Nucl. Instrum. Methods Phys. Res., Sect. A* **618**, 209 (2010).
- [31] B. L. Berman and S. C. Fultz, *Rev. Mod. Phys.* **47**, 713 (1975).
- [32] T. Kondo, H. Utsunomiya, H. Akimune, T. Yamagata, A. Okamoto, H. Harada, F. Kitatani, T. Shima, K. Horikawa, and S. Miyamoto, *Nucl. Instrum. Methods Phys. Res., Sect. A* **659**, 462 (2011).
- [33] J. Allison *et al.*, *IEEE Trans. Nucl. Sci.* **53**, 270 (2006).
- [34] D. M. Filipescu, I. Gheorghe, H. Utsunomiya, S. Goriely, T. Renstrøm, H.-T. Nyhus *et al.*, *Phys. Rev. C* **90**, 064616 (2014).
- [35] H.-T. Nyhus, T. Renstrøm, H. Utsunomiya, S. Goriely, D. M. Filipescu, I. Gheorghe *et al.*, *Phys. Rev. C* **91**, 015808 (2015).
- [36] P. Carlos *et al.*, *Nucl. Phys. A* **258**, 365 (1976).
- [37] B. L. Berman, R. E. Pywell, S. S. Dietrich, M. N. Thompson, K. G. McNeill, and J. W. Jury, *Phys. Rev. C* **36**, 1286 (1987).
- [38] Data extracted using the NNDC On-Line Data Service from the ENSDF Database, November 2014, <http://www.nndc.bnl.gov/ensdf>.
- [39] R. Capote *et al.*, *Nucl. Data Sheets* **110**, 3107 (2009); *R IPL-3 Handbook for Calculation of Nuclear Reaction*, available at <https://www-nds.iaea.org/R IPL-3/>.
- [40] S. F. Mughabghab, *Atlas of Neutron Resonances*, 5th ed. (Elsevier, Amsterdam, 2006).
- [41] T. von Egidy and D. Bucurescu, *Phys. Rev. C* **80**, 054310 (2009).
- [42] M. Guttormsen *et al.*, *Eur. Phys. J. A* **51**, 170 (2015).
- [43] H. K. Toft, A. C. Larsen, U. Agvaanluvsan, A. Bürger, M. Guttormsen, G. E. Mitchell, H. T. Nyhus, A. Schiller, S. Siem, N. U. H. Syed, and A. Voinov, *Phys. Rev. C* **81**, 064311 (2010).
- [44] T. Ericson, *Nucl. Phys.* **11**, 481 (1959).
- [45] T. Ericson, *Adv. Phys.* **9**, 425 (1960).
- [46] Y. Kalmykov, C. Özen, K. Langanke, G. Martínez-Pinedo, P. von Neumann-Cosel, and A. Richter, *Phys. Rev. Lett.* **99**, 202502 (2007).
- [47] S. Hilaire and S. Goriely, *Nucl. Phys. A* **779**, 63 (2006)
- [48] S. Hilaire, J.-P. Delaroche, and M. Girod, *Eur. Phys. J. A* **12**, 169 (2001).
- [49] S. Goriely, S. Hilaire, and A. J. Koning, *Phys. Rev. C* **78**, 064307 (2008).
- [50] A. Gilbert and A. G. W. Cameron, *Can. J. Phys.* **43**, 1446 (1965).
- [51] L. G. Moretto, A. C. Larsen, F. Giacoppo, M. Guttormsen, S. Siem, and A. V. Voinov, *J. Phys.: Conf. Ser.* **580**, 012048 (2015).
- [52] A. Voinov, M. Guttormsen, E. Melby, J. Rekstad, A. Schiller, and S. Siem, *Phys. Rev. C* **63**, 044313 (2001).
- [53] J. Kopecky and M. Uhl, *Phys. Rev. C* **41**, 1941 (1990).
- [54] A. C. Larsen, M. Guttormsen, M. Krtička, E. Běták, A. Bürger, A. Görgen, H. T. Nyhus, J. Rekstad, A. Schiller, S. Siem,

- H. K. Toft, G. M. Tveten, A. V. Voinov, and K. Wikan, *Phys. Rev. C* **83**, 034315 (2011).
- [55] D. Negi *et al.* (unpublished).
- [56] R. Massarczyk, R. Schwengner, L. A. Bernstein, M. Anders, D. Bemmerer, R. Beyer, Z. Elekes, R. Hannaske, A. R. Junghans, T. Kögler, M. Röder, K. Schmidt, A. Wagner, and L. Wagner, *Phys. Rev. C* **92**, 044309 (2015).
- [57] A. Spyrou, S. N. Liddick, A. C. Larsen *et al.*, *Phys. Rev. Lett.* **113**, 232502 (2014).
- [58] D. Zwarts, *Comput. Phys. Commun.* **38**, 365 (1985).
- [59] R. Schwengner, *Phys. Rev. C* **90**, 064321 (2014).
- [60] T. G. Tornyi, M. Guttormsen, T. K. Eriksen, A. Görgen, F. Giacoppo, T. W. Hagen, A. Krasznahorkay, A. C. Larsen, T. Renstrøm, S. J. Rose *et al.*, *Phys. Rev. C* **89**, 044323 (2014).
- [61] F. Käppeler, R. Gallino, S. Bisterzo, and Wako Aoki, *Rev. Mod. Phys.* **83**, 157 (2011).
- [62] Z. Y. Bao *et al.*, *At. Data Nucl. Data Tables* **76**, 70 (2000).
- [63] A. J. Koning, S. Hilaire, and M. C. Duijvestijn, in TALYS-1.6: *Proceedings of the International Conference on Nuclear Data for Science and Technology*, 22–27 April (2007), Nice, France, edited by O. Bersillon, F. Gunsing, E. Bauge, R. Jacqmin, and S. Leray (EDP Sciences, Les Ulis, 2008), pp. 211–214.
- [64] A. Koning and J.-P. Delaroche, *Nucl. Phys. A* **713**, 231 (2003).
- [65] E. Bauge, J. P. Delaroche, and M. Girod, *Phys. Rev. C* **63**, 024607 (2001).
- [66] S. Goriely and E. Khan, *Nucl. Phys. A* **706**, 217 (2002).
- [67] M. Arnould, S. Goriely, and K. Takahashi, *Phys. Rep.* **450**, 97 (2007).
- [68] S. Goriely, N. Chamel, and J. M. Pearson, *Phys. Rev. Lett.* **102**, 152503 (2009).
- [69] S. Goriely, E. Khan, and M. Samyn, *Nucl. Phys. A* **739**, 331 (2004).